ACS PHYSICAL CHEMISTRY Au
AN OPEN ACCESS JOURNAL OF THE AMERICAN CHEMICAL SOCIETY

pubs.acs.org/physchemau
Article

Simple and Efficient Detection Scheme of Two-Color Fluorescence Correlation Spectroscopy for Protein Dynamics Investigation from Nanoseconds to Milliseconds

Yutaka Sano, Yuji Itoh, Supawich Kamonprasertsuk, Leo Suzuki, Atsuhito Fukasawa, Hiroyuki Oikawa,* and Satoshi Takahashi*

Cite This: ACS Phys. Chem Au 2024, 4, 85−93
Read Online

ACCESS | Metrics & More | Article Recommendations | Supporting Information

ABSTRACT: Nanosecond resolved fluorescence correlation spectroscopy (ns-FCS) based on two-color fluorescence detection is a powerful strategy for investigating the fast dynamics of biological macromolecules labeled with donor and acceptor fluorophores. The standard methods of ns-FCS use two single-photon avalanche diodes (SPADs) for the detection of single-color signals (four SPADs for two-color signals) to eliminate the afterpulse artifacts of SPAD at the expense of the efficiency of utilizing photon data in the calculation of correlograms. Herein, we demonstrated that hybrid photodetectors (HPDs) enable the recording of fluorescence photons in ns-FCS based on the minimal system using two HPDs for the detection of two-color signals. However, HPD exhibited afterpulses at a yield with respect to the rate of photodetection ($<10^{-4}$) much lower than that of SPADs ($\sim10^{-2}$), which could still hamper correlation measurements. We demonstrated that the simple subtraction procedure could eliminate afterpulse artifacts. While the quantum efficiency of photodetection for HPDs is lower than that for high-performance SPADs, the developed system can be practically used for two-color ns-FCS in a time domain longer than a few nanoseconds. The fast chain dynamics of the B domain of protein A in the unfolded state was observed using the new method.

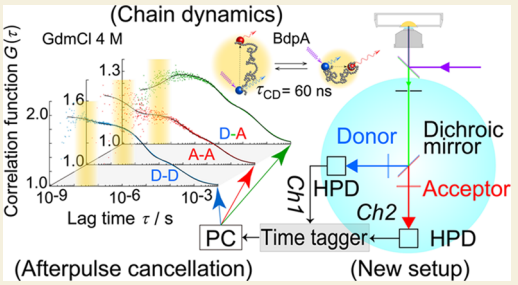

KEYWORDS: *nanosecond fluorescence correlation spectroscopy, hybrid photodetector, afterpulse, B domain of protein A, chain dynamics*

INTRODUCTION

Nanosecond resolved fluorescence correlation spectroscopy (ns-FCS) is a powerful strategy for investigating the fast dynamics of biological macromolecules.[1−5] One example of such dynamics includes a folding transition of proteins, in which the interplay of the secondary structure formation and the collapse of unfolded polypeptides leads to the cooperative formation of folded structures.[6−9] Dynamics can be monitored by labeling donor and acceptor fluorophores to a sample, observing the fluorescence signals of two fluorophores, and calculating the autocorrelation and cross-correlation of their intensity fluctuations. As the donor and acceptor fluorescence intensities are modulated by the Förster resonance energy transfer (FRET) mechanism, the correlations reflect the dynamic changes in the distance between the two fluorophores and their orientations. Furthermore, the photophysical properties of fluorophores, such as the accumulation of the lowest excited triplet (T_1) state, the quenching of the excited singlet (S_1) state by surrounding quenchers, and the rotational dynamics of the fluorophores in the polarization-sensitive setup, can be monitored.[4] The correlation analysis enables the ensemble averaging of photon data in fast time domains shorter than microseconds, where the sparse photons of single fluorophores do not allow the real-time tracking of single-molecule events. Moreover, the method enables the acquisition of information in a wide time domain, from nanoseconds to milliseconds, in single measurements.

However, a limitation exists in the measurement of fluorescence correlation data in the nanosecond region, i.e., artifacts inherent to standard photodetectors, single-photon avalanche diodes (SPADs). Although a SPAD enables a high-speed detection of single photons via the avalanche amplification of photoelectrons in the Geiger mode and their rapid quenching, the main output signals of SPAD are followed by afterpulses in the time domain up to microseconds, adversely affecting the analysis of correlation data.[10−12] In high-performance SPADs used for single-molecule fluorescence spectroscopy (e.g., SPCM-AQRH, Excelitas), the catalogued yield of afterpulse generation with respect to the

Received: August 10, 2023
Revised: October 29, 2023
Accepted: October 30, 2023
Published: November 10, 2023

rate of photon detection is 1%. The yields of afterpulse were known to vary significantly for different detectors in the same model.[13] Accordingly, the fluorescence correlation measurements in the time domain shorter than microseconds require the Hanbury Brown and Twiss optical setup that uses two detectors for the detection of single-color photons that are separated using a beam splitter (four detectors for two-color measurements).[14] In the seminal articles reporting the application of two-color ns-FCS for protein dynamics investigation, the time intervals between two consecutive photons detected by the two detectors were measured by using a time-correlated single-photon counting (TCSPC) board to calculate correlograms down to the picosecond time domain (Figure 1A).[15,16] Recent progress in photon counting

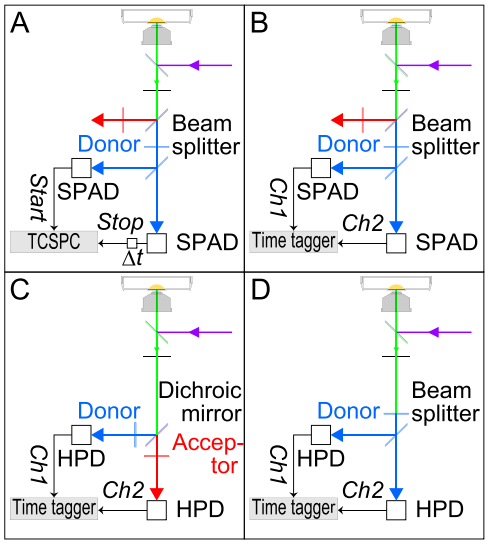

Figure 1. Comparison of the data acquisition schemes of ns-FCS measurements. (A) Hanbury Brown and Twiss optics and two SPADs for the measurement of the time intervals between two consecutive photons. The output signals of SPADs are connected to the start and stop signals of the TCSPC board. The parts required for the acceptor photon measurements are omitted for simplicity. (B) Hanbury Brown and Twiss optics connected to the time-tag counting board. The cross-correlation analysis of the two signals eliminates the afterpulse noises. (C) New proposal for two-color ns-FCS measurements. The donor and acceptor fluorescence signals are separated by a dichroic mirror and detected by using two HPDs. The output signals of the two detectors are recorded using a time-tag counting board. (D) System used herein in the control measurement based on the Hanbury Brown and Twiss optics. Donor fluorescence selected by a bandpass filter was separated by a beam splitter and detected by two HPDs, whose outputs were recorded by a time-tag counting board.

electronics made it possible to conduct a time-tag recording of all of the arrival times of the photons detected by the two detectors (Figure 1B). As the afterpulses of different detectors are not correlated, the cross-correlation analysis of the signals of two detectors can eliminate afterpulse artifacts.[17−19] The cross-correlation method was used in a pioneering investigation based on two counting boards, achieving the picosecond time resolution in the single-color FCS measurement.[20] However, methods based on Hanbury Brown and Twiss optics sacrifice the efficiency of utilizing photons. As the photons are divided into two detectors, only 50% of the total signals are used for the calculation of the correlation functions. Thus, the technique introduced to eliminate the afterpulse artifacts of a SPAD complicates the optics and impedes the efficient measurements of ns-FCS.

Herein, we describe the use of an alternative photodetector, hybrid photodetector (HPD), and time-tag counting board for the ns-FCS measurements without relying on the Hanbury Brown and Twiss setup. HPD achieves the high-efficiency detection of single photons by combining the avalanche photodiode and photomultiplier tube operated in the linear amplification mode.[21−23] While HPD has no detector deadtime, its output pulse duration (∼1 ns) is an effective deadtime when used with a standard photon counting board. The quantum efficiency of GaAsP-type HPD (Hamamatsu Photonics, R10467-40) in the green region (45% at 550 nm) is comparable to that (55% at 550 nm) of high-performance SPAD (Excelitas, SPCM-AQRH) but is lower in the red and far-red regions (30% at 700 nm) compared to that of SPAD (65% at 700 nm). Most importantly, HPDs can eliminate (though not completely as we will discuss later) the afterpulses.[21,22] Thus, HPDs may help construct a simple FCS detection system based on minimum optics using a single detector for single-color detection (Figure 1C). Herein, we discuss the advantages and practical problems of the FCS system based on the HPD detection. We demonstrate that the fast chain dynamics in the unfolded state of doubly labeled protein can be observed based on the current system.

METHODS

Detection System for the Two-Color Fluorescence Correlation Spectroscopy Based on HPDs

We constructed a system for two-color fluorescence correlation measurements, as explained in Supporting Figure S1. In summary, a continuous-wave 484 nm laser (LDS1003, Precise Gauges) was focused on sample solutions using a water immersion objective (UPlanSApo 60x, NA = 1.2, Olympus) via reflection from the first dichroic mirror (MD499, Thorlabs). The fluorescence photons collected using the same objective were passed through the first dichroic mirror and focused on a 50 μm pinhole (P50H, Thorlabs). The donor and acceptor photons selected by the second dichroic mirror (67-083, Edmund) and the bandpass filters in the donor (FBH520-40, Thorlabs) and acceptor (FF01-655/40-25, Semrock) paths were detected by an HPD (H13223-40, Hamamatsu Photonics), whose outputs were amplified (C10778, Hamamatsu Photonics) and recorded using a TCSPC module in the time-tag mode (TimeHarp 260 NANO, PicoQuant). The module was controlled using a software tool (QuCoa, PicoQuant). To obtain the control fluorescence correlation data of rhodamine 110 based on the Hanbury Brown and Twiss optics, we replaced the second dichroic mirror with a beam splitter (BSW10R, Thorlabs) and installed a bandpass filter for rhodamine 110 (MF525-39, Thorlabs) before the splitter (Figure 1D). Moreover, this setup was used to capture excitation light backscattered from the glass to calculate the afterpulse noises of individual HPDs when the focus of the laser was adjusted to be near the coverglass surface.

Sample Preparation

A mutant of the B domain of protein A (BdpA) (K5C/Y15F/A55C) was labeled with Alexa488 (Thermo Fisher) and ATTO633 (ATTO-TEC) using a cysteine−maleimide linkage and purified as previously described.[24] In summary, the protein at 300 μM reacted with a 1.3-fold excess of ATTO633 maleimide and was purified via reversed-phase HPLC on a C18 column. The single-labeled sample adjusted at 200 μM reacted with a 10-fold excess of Alexa488 maleimide and was purified using the reversed-phase HPLC. The fluorescence spectra of the labeled sample excited at 470 nm comprised the donor fluorescence, which peaked at ∼525 nm, and the acceptor fluorescence, which peaked at ∼660 nm, as reported previously.[24]

https://doi.org/10.1021/acsphyschemau.3c00040
ACS Phys. Chem Au 2024, 4, 85−93

The concentration of BdpA was 3 nM for the measurements in the absence and presence of 2 M GdmCl and 15 nM for the measurements in 4 M GdmCl. The measurement buffer adjusted at pH 7.5 comprised 20 mM tris(hydroxymethyl)aminomethane and various concentrations of guanidinium chloride (GdmCl). The photoprotection agent, i.e., 6-hydroxy-2,5,7,8-tetramethylchroman-2-carboxylic acid (Trolox), and the radical scavenger, i.e., cysteamine, at final concentrations of 1 and 10 mM, respectively, were dissolved in the buffer. Following the reported protocol, the buffer in the presence of Trolox and cysteamine was incubated overnight at approximately 22 °C to form a trace amount of Trolox quinone, which can quench the triplet state more efficiently.[25−27] 1 nM rhodamine 110 was prepared in pure water.

Measurements of the Fluorescence Correlations and the Glass Scattering

Glass-base dishes (3971-035, AGC Techno Glass) were used as sample cells, whose inner surface was coated with 2-methacryroyloxyethylphosphorylcholine (MPC) polymer (Lipidure CM5206, NOF) to prevent sample adsorption. For coating, a 0.5% (w/v) solution of MPC in 99.5% ethanol was dropped on the glass surface and dried under vacuum; 500 μL of the sample solution was placed on the dried coated dish and was sealed with parafilm to prevent sample evaporation during the FCS measurements. The ns-FCS measurements were performed in a room at 22 °C. The excitation laser power was roughly estimated near the focus point of the objective with a power meter (PM400, Thorlabs). We measured the arrival times of the donor and acceptor photons simultaneously for 30 min and repeated the measurements multiple times. The total data acquisition times were 8, 7, and 7 h for BdpA in the presence of 0, 2, and 4 M GdmCl, respectively. The optical and electronic systems were stable during these data accumulation periods; however, the sample exhibited gradual breaching in the presence of photoprotection agents. We exchanged samples approximately every 1 h of data accumulation. During the measurement of 3 nM BdpA in the absence of denaturant at a nominal laser power of 100 μW, the total photon fluxes for the donor and acceptor channels were 45.5 and 13.3 ms^{-1}, respectively. For glass-scattering measurements, the scattering of the glass at a nominal excitation power of 800 μW was accumulated for 80 min or 5 h.

Calculation of Fluorescence Correlations and Spike Cancellation

After measuring the photons of the sample or glass scattering, the donor−donor (D−D), acceptor−acceptor (A−A) autocorrelations, and the donor−acceptor (D−A) cross-correlation and their standard deviations were calculated using SymPhoTime64 (PicoQuant), in which the standard deviations were estimated using the bootstrap method. The software divided the lag time of the correlograms from 1 ns to 10 ms into 1008 points so that the time width for each data point was doubled at every 51 data points. If multiple measurements were performed for the same sample under the same conditions, we weight-averaged the individual correlations using the square inverse of the standard deviation for each data point as the weight factor to obtain the final correlations. The correlations calculated were used as the raw correlations of the sample fluorescence modulated by the afterpulse noises of HPD (see below), $G^{HPD}_{sample}(\tau)$, and that of the glass scattering, $G^{HPD}_{scat}(\tau)$. Moreover, we recorded the total photon counts for each measurement and estimated the average photon counting rates, i.e., I_{sample} and I_{scat}, by dividing the total photon counts with the total data accumulation time and used the values for spike cancellation based on eq 5 (see below). The errors of the noise-canceled correlation were estimated based on the error propagation formula derived from eq 5. As the total number of photons used to estimate I_{sample} and I_{scat} was extremely large (typically more than 10^8), their uncertainty based on the photon statistics was several orders of magnitude smaller than the uncertainties of other terms of eq 5. Thus, the uncertainties of I_{sample} and I_{scat} were ignored in the error estimation. To minimize the errors in $G^{HPD}_{scat}(\tau)$, the glass-scattering data of a longer time period should be accumulated. For each HPD unit, we obtained the $G^{HPD}_{scat}(\tau)$ data individually.

Fitting of the Correlation Functions

We measured the correlation data for rhodamine 110 at a nominal excitation power of 100 μW and fit the correlation curve in the time domain longer than 100 ns using eq 1.

$$G(\tau) = G_0 \cdot \frac{1 - F + F \cdot e^{-\tau/\tau_F}}{1 - F} \cdot \frac{1}{1 + \tau/\tau_D} \cdot \frac{1}{\sqrt{1 + s^{-2} \cdot \tau/\tau_D}} + G(\infty) \quad (1)$$

where G_0 denotes the fitted correlation amplitude extrapolated to τ = 0; F denotes the fraction of the triplet state; τ_F and τ_D denote the time constants for triplet state accumulation and translational diffusion, respectively; s denotes the ratio of the axial radius to the radial radius of the measurement volume; and $G(\infty)$ denotes the correlation at τ = ∞ and was set to 1.[28] The estimated s factor was 7.06, which was used as the fixed parameter in fitting the sample correlation data.

For the fitting of the D−D autocorrelation data obtained for the sample after the spike noise cancellation, i.e., $G_{sample,D-D}(\tau)$, we used eq 2.

$$G_{sample,D-D}(\tau) = G_{0,D-D} \cdot (1 + C_{D-D} \cdot e^{-\tau/\tau_{CD}}) \cdot \frac{1 - F_{D-D} + F_{D-D} \cdot e^{-\tau/\tau_{F,D-D}}}{1 - F_{D-D}} \cdot \frac{1}{1 + \tau/\tau_{D,D-D}} \cdot \frac{1}{\sqrt{1 + s^{-2} \cdot \tau/\tau_{D,D-D}}} + G(\infty) \quad (2)$$

where $G_{0,D-D}$ denotes the fitted correlation amplitude in the D−D correlation extrapolated to τ = 0; $G(\infty)$ denotes the correlation at τ = ∞ and was set to 1; C_{D-D} and F_{D-D} denote the amplitudes for the chain dynamics and the triplet state accumulation in the D−D correlation, respectively; $\tau_{F,D-D}$ and $\tau_{D,D-D}$ denote the time constants for the triplet state accumulation and the translational diffusion in the D−D correlation, respectively; and τ_{CD} denotes the time constant for the chain dynamics. Similarly, for the fitting of the A−A autocorrelation after the spike noise cancellation, $G_{sample,A-A}(\tau)$, and the D−A cross-correlation, $G_{sample,D-A}(\tau)$, the variations in eq 2, where suffix D−D was replaced with A−A and D−A, were used.

The D−D, A−A, and D−A correlation data were fitted simultaneously by the respective fitting functions by setting τ_{CD} as a common parameter. We set s with the value estimated by the fitting of the rhodamine 110 data for the D−D, A−A, and D−A correlations. The data points shorter than 5 ns exhibiting the apparent antibunching behavior were excluded from the fitting owing to the small number of data points. The square inverse of the standard deviation of each data point was used as the weighting parameter of fitting. The global fitting routine of the nonlinear least-squares fitting of Igor Pro (WaveMetrics) was used.

Estimation of the Count Rate Per Molecule

The count rate per molecule (CRM) is the number of fluorescence photons emitted from a single fluorophore and detected during a unit time interval. First, the background levels B, mainly attributable to the Raman scattering of water and the detector dark count, for the donor and acceptor channels were measured by using a buffer solution. The B values at a nominal laser power of 100 μW were ∼5 and ∼0.4 counts/ms for the donor and acceptor channels, respectively. The latter was almost the same as the detector's dark count (0.3−0.4 counts/ms). Second, the average number of fluorescent molecules in the observation volume (N) was estimated using eq 3.

$$N = \frac{1}{G_0} \cdot \left(1 - \frac{B}{I_{sample}}\right)^2 \quad (3)$$

where I_{sample} denotes the average photon counting rate and G_0 denotes the correlation amplitude extrapolated to τ = 0 obtained based on the

https://doi.org/10.1021/acsphyschemau.3c00040
ACS Phys. Chem Au 2024, 4, 85−93

fitting of correlation using eq 1 or eq 2. Third, the CRM was calculated by using CRM = $(I_{sample} - B)/N$. The CRM is expressed as the number of photons detected per millisecond per molecule.

RESULTS AND DISCUSSION

HPD Exhibited Unexpected Afterpulses

We constructed an FCS measurement system based on the confocal setup and based on single-color excitation and two-color detection as explained in the Methods section and Supporting Figure S1. A continuous-wave laser at 484 nm was introduced to a water immersion objective and focused on a sample solution. The fluorescence photons emitted were collected using the same objective, separated into the donor and acceptor photons, and detected using two HPDs. The output signals of the HPDs were amplified and recorded by a time-tag counting board. The initial trials of the FCS measurements based on the constructed system exhibited unexpected spike-shaped noises in the autocorrelation data of rhodamine 110 (pink, Figure 2A). The correlation data obtained for the donor channel exhibited a standard decay in the time domain longer than 10 μs, reflecting a diffusion of the fluorophore and a phase from 100 ns to 10 μs corresponding to the triplet state accumulation. In contrast, the nonnegligible amplitude of noises was observed in the time domain from 10 to 100 ns. The data points in the time domain shorter than 10 ns were scattered; however, the scattered data were detected reproducibly in different measurements and appeared as spikes. We found that the spikes were caused by the low-yield afterpulses of HPD. Except for one conference proceeding describing the afterpulse in the older model of HPD,[29] previous studies reported the absence of the afterpulse phenomenon for HPDs.[21,22] The correlation data shown in orange in Figure 2A were obtained by measuring the noncorrelated scattering of glass and demonstrated the same spike-shaped noises, including the time domain shorter than 10 ns. The data illustrated in Supporting Figure S2 indicated that the HPD after the detection of single photons demonstrated single pulses at time zero. However, at a very low yield (less than 1×10^{-4}), the second pulses followed the first pulses after the time intervals of a few nanoseconds. The shape of the second pulses was indistinguishable from that of the main pulses.

A plausible origin of afterpulses is ion feedback in the photomultiplier unit of an HPD. The HPD comprises a photocathode, vacuum photomultiplier, and avalanche diode.[23] Upon the detection of photons, the photoelectrons emitted from the photocathode are accelerated in the vacuum tube and create holes in the diode unit. However, the remaining gases in the tube may be ionized upon rare collisions with photoelectrons and generate positive ions that return to and collide with the photocathode, causing delayed pulses. The afterpulses could not be eliminated by changing the operational setting of the HPD, such as the acceleration voltage or the bias voltage, or by changing the pulse discrimination setting of the counting board (not demonstrated). The rate and delay patterns of the noises appeared reproducibly (not demonstrated). A few HPD units generated smaller noise; however, it was difficult to determine an HPD unit without noise.

The artifacts caused by afterpulses can be eliminated using the subtraction method proposed previously.[12] We assume that photons are detected at a very low rate, and only a single photon at most is detected at a time. In addition, we assume

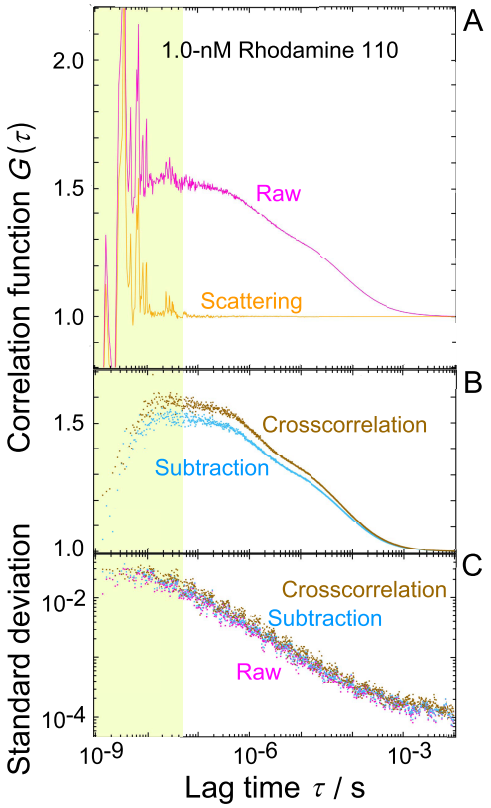

Figure 2. Fluorescence correlation data obtained for rhodamine 110. The nominal laser excitation was 400 μW. (A) Pink trace represents the raw autocorrelation data of rhodamine 110 obtained using the developed system (Figure 1C). The measurement was conducted at an average photon counting rate of 96 ms^{-1}. The orange trace represents the autocorrelation data of the glass scattering (orange). (B) Blue dots represent the correlation of rhodamine 110, in which the afterpulse spikes in the raw data (pink in panel A) are subtracted using the data obtained by the scattering measurements (orange in (A)). The brown dots represent the correlation data of rhodamine 110 obtained using Hanbury Brown and Twiss optics and two HPDs (Figure 1D) based on the cross-correlation analysis. The photon counting rates of the two detectors are 50 and 58 ms^{-1}. (C) Comparison of the standard deviation (pink) for the raw autocorrelation of rhodamine 110 (pink in (A)) obtained using the developed system (Figure 1C) and that (blue) for the noise-canceled autocorrelation performed using the subtraction method (blue in (B)). The standard deviations (brown) for the noise-canceled correlation obtained using the cross-correlation method (brown in (B)) were exhibited as well. Ordinate and abscissa are presented in the logarithmic scale. The stepwise reduction in the standard deviation was caused by the stepwise increase in the time width allotted to each data point (Methods section).

that the yield of the afterpulse generation is low. The autocorrelation ($G^{HPD}_{sample}(\tau)$) of the apparent sample signal measured using an HPD, i.e., the sum of the true sample signal and the afterpulse signal, can be related to the autocorrelation of the true sample signal ($G_{sample}(\tau)$) as follows

$$G^{HPD}_{sample}(\tau) = G_{sample}(\tau) + \frac{\Delta t}{I_{sample}} \cdot \alpha(\tau) \quad (4)$$

where $\alpha(\tau)$ denotes the afterpulse yield of HPD as a function of the time after the detection of real photons, Δt denotes the time window of correlation, and I_{sample} denotes the average photon counting rate for the sample data.[12] The contribution

https://doi.org/10.1021/acsphyschemau.3c00040
ACS Phys. Chem Au 2024, 4, 85−93

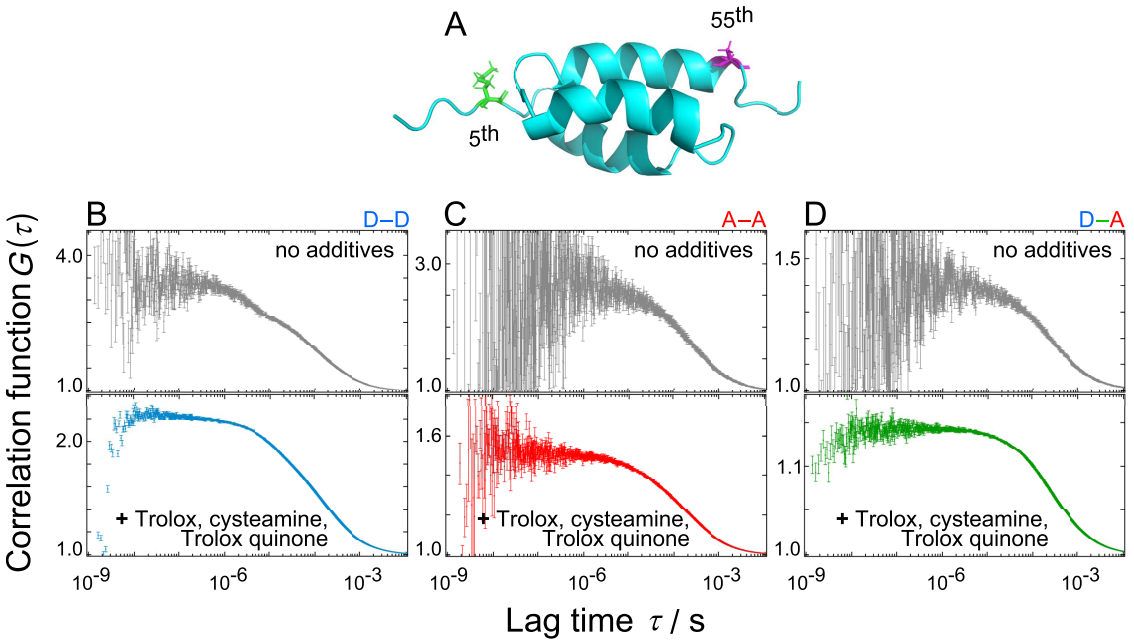

Figure 3. Fluorescence correlation data were obtained for BdpA in the absence of a denaturant. (A) Folded structure of the BdpA determined via NMR spectroscopy (PDB ID: 1BDD).[31] The 5th and 55th residues were replaced with cysteine and labeled with Alexa488 and ATTO633. The figure was prepared by using PyMOL. (B–D) Autocorrelation is calculated for the donor fluorescence fluctuation (B), autocorrelation is calculated for the acceptor fluctuation (C), and cross-correlation is calculated for the donor and acceptor fluctuation (D). The upper and lower traces correspond to the sample measured in the absence and presence of photoprotection agents, which are 1 mM Trolox, 10 mM cysteamine, and a trace amount of Trolox quinone. For the data in the absence and presence of the photoprotection agents, the protein concentrations are 1.5 and 3 nM, respectively. The nominal laser power is 100 μW.

of $\alpha(\tau)$ can be evaluated and subtracted from eq 4 by measuring the autocorrelation of noncorrelated photons, such as glass scattering ($G_{\mathrm{scat}}^{\mathrm{HPD}}(\tau)$), detected by the same HPD unit using the following equation:

$$G_{\mathrm{sample}}(\tau) = G_{\mathrm{sample}}^{\mathrm{HPD}}(\tau) - \frac{I_{\mathrm{scat}}}{I_{\mathrm{sample}}} \cdot \{G_{\mathrm{scat}}^{\mathrm{HPD}}(\tau) - 1\},\ \tau \neq 0 \quad (5)$$

where I_{scat} denotes the average photon counting rate for the scattering data. Equation 5 is valid for τ longer than the duration of a single output pulse of HPD (~1 ns). Equations 4 and 5 were derived assuming that the average photon counting rates, i.e., I_{sample} and I_{scat}, do not change over the data accumulation period.[12] The rates might vary gradually in the actual measurements due to unavoidable changes in the experimental conditions, such as the sample concentration. However, the changes do not affect the noise cancellation procedure, and I_{sample} and I_{scat} can be estimated from the total number of detected photons divided by the total accumulation period (see the Methods section).

Figure 2B shows the subtracted correlation (blue) for rhodamine 110 based on eq 5 demonstrating a clear cancellation of the afterpulse artifacts. Unexpectedly, the cancellation revealed a dip in the time domain shorter than 5 ns, which is reminiscent of an antibunching phenomenon detected for fluorescence photons emitted from a single fluorophore. A single fluorophore after the fluorescence emission might be immediately excited to the S_1 state but stays in S_1 before the emission of the second fluorescence photon, causing an antibunching corresponding to the lifetime of the S_1 state. However, the observed antibunching is likely ascribed to the dead time of the time-tag board (<2 ns) and partially to the S_1 state lifetime of the fluorophore. To confirm the correlation data thus obtained, we conducted a control measurement using the Hanbury Brown and Twiss optics and the time-tag detection of fluorescence photons of rhodamine 110 using two HPDs after separation by a half-mirror (Figure 1D). As the afterpulses of different detectors are not correlated, the cross-correlation analysis of the two signals canceled the spikes and enabled the observation of the correlation of rhodamine 110 (brown, Figure 2B). The coincidence of the two data sets rationalized the proposed data acquisition and the spike cancellation procedures. The parameters obtained based on the fitting of the two rhodamine 110 data sets using eq 1 further rationalized the data acquisition and analysis schemes (Supporting Table S1).

Figure 2C presents the standard deviation values for each data point of the correlations obtained by the current system based on a single HPD (Figure 1C) before (pink) and after (blue) the subtraction of the afterpulse artifacts and by the Hanbury Brown and Twiss system based on two HPDs (Figure 1D) after the cross-correlation analysis (brown). The two measurements were conducted for the same sample solution of rhodamine 110 adjusted at 1.0 nM, the same laser power (the nominal power of 400 μW), and the data accumulation time (20 min). The data for the subtraction calculation were obtained at an average photon detection rate of 96 ms^{-1} for the single detector (Figure 1C). The data for the cross-correlation calculation were obtained at 50 and 58 ms^{-1} for the two detectors, as the photon signal was separated using the beam splitter (Figure 1D). The raw data before the spike subtraction exhibited the lowest errors (pink). This is because the standard deviations of the correlations at shorter lag times are determined by the photon shot noises, which are inversely proportional to the square root of the photon numbers.[30] The subtraction of the spike noises increased the error levels due to

https://doi.org/10.1021/acsphyschemau.3c00040
ACS Phys. Chem Au 2024, 4, 85–93

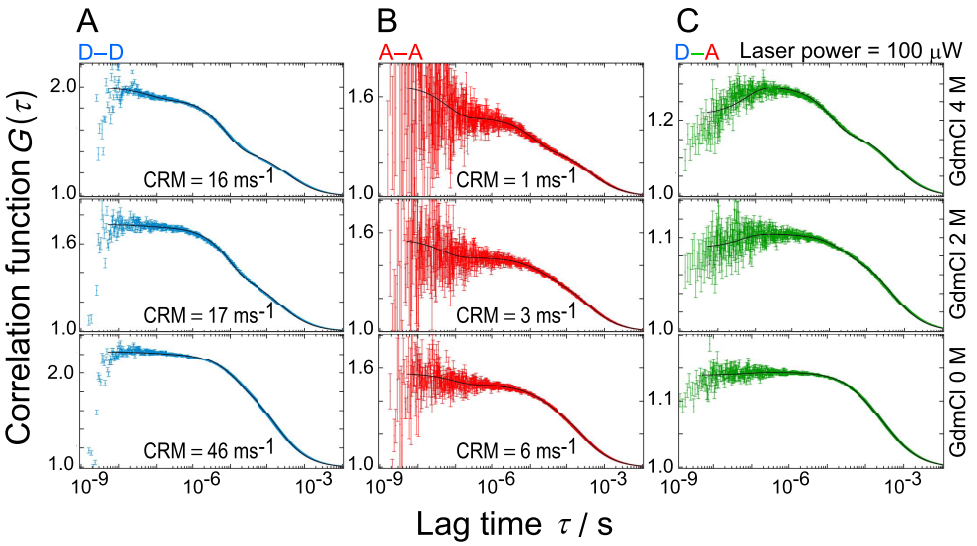

Figure 4. Fluorescence correlation data for the equilibrium unfolding transition of BdpA in the absence and presence of 2 and 4 M GdmCl. For all of the measurements, the laser excitation power is 100 μW. All data are obtained in the presence of photoprotection agents. (A) D−D autocorrelations are calculated based on the donor fluorescence data. (B) A−A autocorrelations are calculated based on the acceptor fluorescence data. (C) D−A cross-correlations are calculated based on the donor and acceptor fluorescence data. The first, second, and third traces from the bottom of each panel corresponded to the sample in the absence and presence of 2 and 4 M GdmCl, respectively. The standard deviation values of all of the data points are presented. The black lines represent the fitted lines obtained based on the global fitting of the D−D, A−A, and D−A correlations based on eq 2 setting τ_{CD} as the global fitting parameter. The data in the absence of GdmCl are the same as those illustrated in Figure 3.

the propagation of the errors in the spike data. However, the noise level after the subtraction (blue) was lower compared to the Hanbury Brown−Twiss system after the cross-correlation calculation (brown). Thus, the simplicity of the developed system using one detector for single-color detection and the comparable signal-to-noise ratio based on the efficient utilization of photons make the current method a practical choice for FCS measurements in time domains longer than a few nanoseconds.

Photophysics and Chain Dynamics of the Doubly Labeled BdpA

Next, we examined the BdpA as an example of doubly labeled proteins, which is a 60-residue three-helix bundle possessing helix 1 from residue 10 to 19, helix 2 from 25 to 37, and helix 3 from 42 to 56 (Figure 3A).[24,31−33] The BdpA is a part of protein A, which is a cell wall protein of *Staphylococcus aureus* and binds to mammalian immunoglobulin G.[31] Owing to its simple structure, the folding mechanism of BdpA has been investigated extensively. We previously labeled the sample with Alexa488 and ATTO633 at the fifth and 55th cysteines and monitored its equilibrium unfolding via fluorescence spectroscopy.[24] While the sample exhibited apparent two-state unfolding when monitored by the ensemble fluorescence measurements, the single-molecule FRET data exhibited heterogeneity in the unfolded state and deviation from simple two-state unfolding. Even in the high-speed tracking of the single-molecule data at the time resolution of several tens of microseconds, the unfolded sample did not exhibit the FRET efficiency fluctuations, suggesting that the dynamics of the unfolded protein chain, if any, should appear at time scales much faster than 10 μs.

We first measured the labeled BdpA under the buffer conditions in the absence of a denaturant, which stabilizes the folded structure. The correlation data of the sample after noise cancellation are presented in Figure 3, in which panels B, C, and D correspond to the D−D autocorrelation, the A−A autocorrelation, and the D−A cross-correlation, respectively. The upper and lower traces in each panel were obtained in the absence and presence, respectively, of 1 mM Trolox, 10 mM cysteamine, and a trace amount of Trolox quinone.[25−27] In the absence of these agents, the correlation data were of low quality due to low fluorescence detection rates of ∼4 and ∼1 ms^{-1} for the donor and acceptor, respectively, at the protein concentration of 1.5 nM. The addition of the agents considerably increased the fluorescence detection rates (∼45 and ∼13 ms^{-1} for the donor and acceptor, respectively, at the protein concentration of 3 nM), and improved the signal-to-noise ratio of the correlations. The agents promote the conversion of T_1 to S_0 of the fluorophores and accelerate their excitation−emission photocycle.[25−27] The data obtained in the presence of the protection agents can be interpreted by assuming a stable structure of BdpA in the native state, as the D−D, A−A, and D−A correlations in the time domain from 10 ns to 1 μs were nearly flat. The quality of the A−A correlation was apparently poorer than that of the D−D correlogram due to the lower quantum efficiency for the photodetection of the HPD in the fluorescence wavelength region of ATTO633 (620−830 nm). However, the data demonstrated that the current system enables the practical acquisition of the correlation data of doubly labeled protein in the time domain from a few nanoseconds to a few milliseconds.

To characterize the folding transition of BdpA, we conducted ns-FCS measurements of BdpA at different concentrations of guanidinium hydrochloride (GdmCl) in the presence of photoprotection agents (Figure 4). The previous ensemble fluorescence data indicated that the GdmCl unfolding of the sample occurred cooperatively with the unfolding free energy difference (ΔG_0) of 4.3 ± 0.6 kcal/mol and the unfolding midpoint ($[GdmCl]_{1/2}$) of 2.9 ± 0.6 M.[24] These values indicated that the sample in the ensemble two-

https://doi.org/10.1021/acsphyschemau.3c00040
ACS Phys. Chem Au 2024, 4, 85−93

Table 1. Time Constants and Amplitudes Obtained by Fitting the Correlation Data for BdpA in the Presence of Various Concentrations of GdmCl[a]

[GdmCl]		0 M	2 M	4 M
τ_{CD}/ns (C)[b]	D−D	80 ± 10 (0.016 ± 0.003)	44 ± 8 (0.021 ± 0.012)	60 ± 10 (0.12 ± 0.02)
	A−A	80 ± 10 (0.13 ± 0.01)	44 ± 8 (0.26 ± 0.02)	60 ± 10 (0.40 ± 0.04)
	D−A	80 ± 10 (−0.03 ± 0.02)[c]	44 ± 8 (−0.14 ± 0.07)[c]	60 ± 10 (−0.26 ± 0.05)[c]
τ_F/μs (F)[b]	D−D	13 ± 1 (0.25 ± 0.01)	9.4 ± 0.5 (0.47 ± 0.01)	8.0 ± 0.6 (0.53 ± 0.02)
	A−A	20 ± 3 (0.18 ± 0.02)	18 ± 4 (0.24 ± 0.02)	12 ± 3 (0.39 ± 0.03)
	D−A	80 ± 60 (0.16 ± 0.1)	23 ± 20 (0.21 ± 0.09)	11 ± 3 (0.41 ± 0.05)
τ_D/μs	D−D	165 ± 3	210 ± 10	310 ± 30
	A−A	230 ± 10	330 ± 30	380 ± 60
	D−A	400 ± 100	500 ± 100	500 ± 100

[a]D−D and A−A autocorrelations and D−A cross-correlation obtained in the presence of various concentrations of GdmCl presented in Figure 4 are globally fitted using eq 2, assuming τ_{CD} as the global fitting parameter. Other parameters are assumed to be independent for D−D, A−A, and D−A. [b]Values in the parentheses denote the relative amplitudes. [c]Negative amplitudes denote the increasing phase of the correlogram.

state scheme was 10% and 95% unfolded at 2 and 4 M GdmCl, respectively. As we discussed, the sample in the absence of GdmCl did not exhibit detectable dynamics in our measurement (Figure 3). In contrast, the increase in the GdmCl concentration caused two significant changes in the correlograms. First, a decay phase with a time constant at approximately 10 μs was detected for all of the D−D, A−A, and D−A correlations. Second, another phase was detected in the time domain shorter than 100 ns. We discuss the two observations in turn.

First, the new decay phase observed at approximately 10 μs in all of the correlograms of BdpA in the presence of GdmCl can be assigned to T_1 accumulation. In standard FCS measurements based on single-color excitation and single-color detection, a fluorophore in the focus volume repeats the excitation and emission photocycle between S_0 and S_1 many times but occasionally converts from S_1 into T_1 via intersystem crossing, causing transient darkening of the fluorophore and a decay phase in fluorescence correlation curves. The decay phase was determined based on multiple factors, including the excitation power, the rate of intersystem crossing, and the quenching of T_1 by molecular oxygen and other quenchers; however, it appeared at approximately 10 μs. To confirm the assignment, we examined the laser power dependency of the correlograms in the presence of 4 M GdmCl (Supporting Figure S3). The amplitude of the 10 μs phase for the D−D, A−A, and D−A correlations increased with an increase in the excitation power. In addition, the time constants became faster at higher laser intensity (Supporting Table S2). These observations are consistent with the larger and faster accumulation of T_1 in the absence of the protection agents. Thus, the phase observed at approximately 10 μs can be assigned to the T_1 accumulation.

The T_1 phase was detected in the D−A cross-correlation of the current measurements based on the single-laser excitation and two-color detection. This is in contrast to the common FCS observations based on two-laser excitation and two-color detection, in which the T_1 states of the two fluorophores accumulate independently and the cross-correlation between the emissions of the two fluorophores does not exhibit the T_1 amplitude. In the current measurements, a photocycle starts from donor excitation followed by either donor emission or energy transfer to the acceptor and its emission. The cycle might be repeated or be occasionally interrupted by the intersystem crossing from S_1 to T_1 of the donor, causing a simultaneous darkening of donor and acceptor fluorophores and creating the T_1 decay phase in the D−A cross-correlation. The amplitude of the T_1 phase in the D−A correlation was less pronounced in the native state because its higher FRET efficiency (E = 0.78 at 0 M GdmCl) compared to the unfolded state (E = 0.53 at 4 M GdmCl)[24] reduced the conversion rate of the donor from S_1 to T_1.

Second, the new phase was detected in the time domain from 10 to 100 ns in the correlations detected in the presence of 4 M GdmCl. While the A−A autocorrelation was noisy, the D−D autocorrelation and D−A cross-correlation exhibited decreasing and increasing trends, respectively, in this time domain, demonstrating anticorrelated changes in the donor and acceptor fluorescence intensities caused by the changes in the FRET efficiency. The phase mainly reflects the chain dynamics of unfolded polypeptides.[15,16] The time constant of the phase obtained based on the global fitting of the correlation data at 4 M GdmCl was 60 ± 10 ns (Table 1). The previous single-molecule FRET investigation exhibited that different molecules of BdpA in its unfolded state exhibit slightly different FRET efficiencies that are mostly constant over the observation time of a few milliseconds.[7,24] The fast chain dynamics observed in the current measurements indicate that each unfolded BdpA having different FRET efficiencies fluctuates on faster time scales. While less obvious, the correlograms obtained in the presence of 2 M GdmCl could be fitted by assuming the chain dynamics phase at a time constant of 44 ± 8 ns (Table 1). The phase might be assigned to the chain dynamics of the unfolded state fraction that is present at ∼10% under this solution condition. Further detailed investigations are required to understand the hierarchy and apparent heterogeneity in the unfolded state dynamics of BdpA.

CONCLUSIONS

We demonstrated that the use of HPD simplified the detection system for the two-color FCS and enabled an efficient utilization of the photon data for the calculation of correlograms in the time domain longer than a few nanoseconds. An HPD is a sensitive and high-fidelity photodetector; however, the output pulses were found to be contaminated with afterpulses occurring at a very low ratio ($<10^{-4}$). We exhibited that afterpulse artifacts can be canceled by considering noncorrelated scattering and subtracting scattering data from fluorescence data. While the lower quantum efficiency of HPDs at longer wavelength regions degrades the quality of acceptor correlations, the developed

https://doi.org/10.1021/acsphyschemau.3c00040
ACS Phys. Chem Au 2024, 4, 85−93

system, using only one detector for single-color detection, enables efficient data utilization for two-color ns-FCS. The system indicated that BdpA in the unfolded state exhibited fast chain dynamics at a time constant of 60 ± 11 ns. As an HPD can detect a large number of photons, the system may be suited for experiments allowing a large photon flux, such as nanophotonic excitation.[34]

■ ASSOCIATED CONTENT

Supporting Information

The Supporting Information is available free of charge at https://pubs.acs.org/doi/10.1021/acsphyschemau.3c00040.

Fitting parameters obtained through the analysis of the FCS correlations for rhodamine 110 and BdpA (Tables S1 and S2); optical setup of the ns-FCS measurements, response of HPD upon the detection of single photons, and correlograms of BdpA in the presence of 4 M GdmCl observed at different excitation laser powers (Figures S1−S3) (PDF)

■ AUTHOR INFORMATION

Corresponding Authors

Hiroyuki Oikawa − *Institute of Multidisciplinary Research for Advanced Materials, Tohoku University, Sendai, Miyagi 980-8577, Japan; Department of Chemistry, Graduate School of Sciences, Tohoku University, Sendai, Miyagi 980-8578, Japan; Graduate School of Life Sciences, Tohoku University, Sendai, Miyagi 980-8577, Japan; MOLCURE, Kawasaki, Kanagawa 212-0032, Japan;* orcid.org/0000-0001-5216-0813; Email: oikawa@molcure.io

Satoshi Takahashi − *Institute of Multidisciplinary Research for Advanced Materials, Tohoku University, Sendai, Miyagi 980-8577, Japan; Department of Chemistry, Graduate School of Sciences, Tohoku University, Sendai, Miyagi 980-8578, Japan; Graduate School of Life Sciences, Tohoku University, Sendai, Miyagi 980-8577, Japan;* orcid.org/0000-0003-1506-9222; Email: satoshi.takahashi.a6@tohoku.ac.jp

Authors

Yutaka Sano − *Institute of Multidisciplinary Research for Advanced Materials, Tohoku University, Sendai, Miyagi 980-8577, Japan; Department of Chemistry, Graduate School of Sciences, Tohoku University, Sendai, Miyagi 980-8578, Japan*

Yuji Itoh − *Institute of Multidisciplinary Research for Advanced Materials, Tohoku University, Sendai, Miyagi 980-8577, Japan; Department of Chemistry, Graduate School of Sciences, Tohoku University, Sendai, Miyagi 980-8578, Japan; Graduate School of Life Sciences, Tohoku University, Sendai, Miyagi 980-8577, Japan;* orcid.org/0000-0002-6699-8665

Supawich Kamonprasertsuk − *Institute of Multidisciplinary Research for Advanced Materials, Tohoku University, Sendai, Miyagi 980-8577, Japan; Department of Chemistry, Graduate School of Sciences, Tohoku University, Sendai, Miyagi 980-8578, Japan*

Leo Suzuki − *Institute of Multidisciplinary Research for Advanced Materials, Tohoku University, Sendai, Miyagi 980-8577, Japan; Graduate School of Life Sciences, Tohoku University, Sendai, Miyagi 980-8577, Japan*

Atsuhito Fukasawa − *Electron Tube Division, Hamamatsu Photonics K. K., Iwata, Shizuoka 438-0193, Japan*

Complete contact information is available at: https://pubs.acs.org/10.1021/acsphyschemau.3c00040

Author Contributions

Y.S., H.O., and S.T. designed the experiments. H.O. designed and constructed the ns-FCS system. Y.S., S.K., L.S., and H.O. performed the ns-FCS experiments. H.O. and Y.I. labeled and purified the sample. A.F. examined the HPD response. Y.S., Y.I., S.K., L.S., H.O., and S.T. analyzed the data. Y.S., Y.I., H.O., and S.T. wrote the paper. All authors have given approval to the final version of the manuscript. CRediT: **Yutaka Sano** formal analysis, investigation, methodology, visualization, writing-original draft, writing-review & editing; **Yuji Itoh** formal analysis, investigation, writing-original draft, writing-review & editing; **Supawich Kamonprasertsuk** investigation; **Leo Suzuki** investigation; **Atsuhito Fukasawa** data curation, formal analysis, investigation; **Hiroyuki Oikawa** conceptualization, data curation, formal analysis, funding acquisition, investigation, methodology, project administration, resources, software, supervision, validation, visualization, writing-original draft, writing-review & editing; **Satoshi Takahashi** conceptualization, formal analysis, funding acquisition, investigation, methodology, project administration, resources, software, supervision, validation, visualization, writing-original draft, writing-review & editing.

Notes

The authors declare no competing financial interest.

■ ACKNOWLEDGMENTS

H.O. is grateful for JSPS KAKENHI Grants JP19K06577, and S.T. for Grants JP20K21166 and JP21H02438. S.T. is also grateful for JST CREST JPMJCR20H8.

■ ABBREVIATIONS

ns-FCS, nanosecond resolved fluorescence correlation spectroscopy; FRET, Förster resonance energy transfer; SPAD, single-photon avalanche diode; TCSPC, time-correlated single-photon counting; HPD, hybrid photodetector; BdpA, B domain of protein A; GdmCl, guanidinium chloride; Trolox, 6-hydroxy-2,5,7,8-tetramethylchroman-2-carboxylic acid; MPC, 2-methacryroyloxyethylphosphorylcholine

■ REFERENCES

(1) Price, E. S.; Aleksiejew, M.; Johnson, C. K. FRET-FCS Detection of Intralobe Dynamics in Calmodulin. *J. Phys. Chem. B* **2011**, *115* (29), 9320−9326.

(2) Felekyan, S.; Sanabria, H.; Kalinin, S.; Kühnemuth, R.; Seidel, C. A. M. Analyzing Förster Resonance Energy Transfer with Fluctuation Algorithms. In *Methods in Enzymology*; Elsevier, 2013; Vol. *519*, pp 39−85.

(3) Sahoo, H.; Schwille, P. FRET and FCS—Friends or Foes? *ChemPhysChem* **2011**, *12* (3), 532−541.

(4) Ghosh, A.; Enderlein, J. Advanced Fluorescence Correlation Spectroscopy for Studying Biomolecular Conformation. *Curr. Opin. Struct. Biol.* **2021**, *70*, 123−131.

(5) Lerner, E.; Barth, A.; Hendrix, J.; Ambrose, B.; Birkedal, V.; Blanchard, S. C.; Börner, R.; Sung Chung, H.; Cordes, T.; Craggs, T. D.; Deniz, A. A.; Diao, J.; Fei, J.; Gonzalez, R. L.; Gopich, I. V.; Ha, T.; Hanke, C. A.; Haran, G.; Hatzakis, N. S.; Hohng, S.; Hong, S. C.; Hugel, T.; Ingargiola, A.; Joo, C.; Kapanidis, A. N.; Kim, H. D.; Laurence, T.; Lee, N. K.; Lee, T. H.; Lemke, E. A.; Margeat, E.; Michaelis, J.; Michalet, X.; Myong, S.; Nettels, D.; Peulen, T. O.; Ploetz, E.; Razvag, Y.; Robb, N. C.; Schuler, B.; Soleimaninejad, H.; Tang, C.; Vafabakhsh, R.; Lamb, D. C.; Seidel, C. A.; Weiss, S. FRET-

Based Dynamic Structural Biology: Challenges, Perspectives and an Appeal for Open-Science Practices. *eLife* **2021**, *10*, No. e60416.
(6) Bhatia, S.; Udgaonkar, J. B. Heterogeneity in Protein Folding and Unfolding Reactions. *Chem. Rev.* **2022**, *122* (9), 8911−8935.
(7) Takahashi, S.; Yoshida, A.; Oikawa, H. Hypothesis: Structural Heterogeneity of the Unfolded Proteins Originating from the Coupling of the Local Clusters and the Long-Range Distance Distribution. *Biophys. Rev.* **2018**, *10* (2), 363−373.
(8) Petrosyan, R.; Narayan, A.; Woodside, M. T. Single-Molecule Force Spectroscopy of Protein Folding. *J. Mol. Biol.* **2021**, *433* (20), No. 167207.
(9) Ferreiro, D. U.; Komives, E. A.; Wolynes, P. G. Frustration, Function and Folding. *Curr. Opin. Struct. Biol.* **2018**, *48*, 68−73.
(10) Burstyn, H. C. Afterpulsing Effects in Photon Correlation Experiments. *Rev. Sci. Instrum.* **1980**, *51* (10), 1431−1433.
(11) Overbeck, E.; Sinn, C.; Flammer, I.; Rička, J. Silicon Avalanche Photodiodes as Detectors for Photon Correlation Experiments. *Rev. Sci. Instrum.* **1998**, *69* (10), 3515−3523.
(12) Zhao, M.; Jin, L.; Chen, B.; Ding, Y.; Ma, H.; Chen, D. Afterpulsing and Its Correction in Fluorescence Correlation Spectroscopy Experiments. *Appl. Opt.* **2003**, *42* (19), 4031−4036.
(13) Ziarkash, A. W.; Joshi, S. K.; Stipčević, M.; Ursin, R. Comparative Study of Afterpulsing Behavior and Models in Single Photon Counting Avalanche Photo Diode Detectors. *Sci. Rep.* **2018**, *8* (1), No. 5076.
(14) Brown, R. H.; Twiss, R. Q. Correlation between Photons in Two Coherent Beams of Light. *Nature* **1956**, *177* (4497), 27−29.
(15) Nettels, D.; Gopich, I. V.; Hoffmann, A.; Schuler, B. Ultrafast Dynamics of Protein Collapse from Single-Molecule Photon Statistics. *Proc. Natl. Acad. Sci. U.S.A.* **2007**, *104* (8), 2655−2660.
(16) Nettels, D.; Hoffmann, A.; Schuler, B. Unfolded Protein and Peptide Dynamics Investigated with Single-Molecule FRET and Correlation Spectroscopy from Picoseconds to Seconds. *J. Phys. Chem. B* **2008**, *112* (19), 6137−6146.
(17) Bendjaballah, C. Autocorrelation Function of Scattered Light for a Binary Fluid near the Critical Mixing Point. *Opt. Commun.* **1973**, *9* (3), 279−282.
(18) Burstyn, H. C.; Sengers, J. V. Time Dependence of Critical Concentration Fluctuations in a Binary Liquid. *Phys. Rev. A* **1983**, *27* (2), 1071−1085.
(19) Vishvakarma, V.; Engberg, O.; Huster, D.; Maiti, S. The Effect of Cholesterol on Highly Curved Membranes Measured by Nanosecond Fluorescence Correlation Spectroscopy. *Methods Appl. Fluoresc.* **2022**, *10* (4), No. 044006.
(20) Felekyan, S.; Kühnemuth, R.; Kudryavtsev, V.; Sandhagen, C.; Becker, W.; Seidel, C. A. M. Full Correlation from Picoseconds to Seconds by Time-Resolved and Time-Correlated Single Photon Detection. *Rev. Sci. Instrum.* **2005**, *76* (8), No. 083104.
(21) Michalet, X.; Cheng, A.; Antelman, J.; Suyama, M.; Arisaka, K.; Weiss, S. In *Hybrid Photodetector for Single-Molecule Spectroscopy and Microscopy*, Proceedings Volume 6862, Single Molecule Spectroscopy and Imaging, 2008; 68620F.
(22) Becker, W.; Su, B.; Holub, O.; Weisshart, K. FLIM and FCS Detection in Laser-Scanning Microscopes: Increased Efficiency by GaAsP Hybrid Detectors. *Microsc. Res. Technol.* **2011**, *74* (9), 804−811.
(23) Yokota, H.; Fukasawa, A.; Hirano, M.; Ide, T. Low-Light Photodetectors for Fluorescence Microscopy. *Appl. Sci.* **2021**, *11* (6), 2773.
(24) Oikawa, H.; Kamagata, K.; Arai, M.; Takahashi, S. Complexity of the Folding Transition of the B Domain of Protein A Revealed by the High-Speed Tracking of Single-Molecule Fluorescence Time Series. *J. Phys. Chem. B* **2015**, *119* (20), 6081−6091.
(25) Cordes, T.; Vogelsang, J.; Tinnefeld, P. On the Mechanism of Trolox as Antiblinking and Antibleaching Reagent. *J. Am. Chem. Soc.* **2009**, *131* (14), 5018−5019.
(26) Ha, T.; Tinnefeld, P. Photophysics of Fluorescent Probes for Single-Molecule Biophysics and Super-Resolution Imaging. *Annu. Rev. Phys. Chem.* **2012**, *63* (1), 595−617.
(27) Campos, L. A.; Liu, J.; Wang, X.; Ramanathan, R.; English, D. S.; Muñoz, V. A Photoprotection Strategy for Microsecond-Resolution Single-Molecule Fluorescence Spectroscopy. *Nat. Methods* **2011**, *8* (2), 143−146.
(28) Schwille, P.; Kummer, S.; Heikal, A. A.; Moerner, W. E.; Webb, W. W. Fluorescence Correlation Spectroscopy Reveals Fast Optical Excitation-Driven Intramolecular Dynamics of Yellow Fluorescent Proteins. *Proc. Natl. Acad. Sci. U.S.A.* **2000**, *97* (1), 151−156.
(29) Saito, T. Y.; Shayduk, M.; Fonseca, M. V.; Hayashida, M.; Lorenz, E.; Mannheim, K.; Mirzoyan, R.; Schweizer, T.; Teshima, M. Recent Progress of GaAsP HPD Development for the MAGIC Telescope Project, arXiv:0709.2052 (Astrophysics), 2007. http://arxiv.org/abs/0709.2052 (accessed Oct 23, 2023).
(30) Saffarian, S.; Elson, E. L. Statistical Analysis of Fluorescence Correlation Spectroscopy: The Standard Deviation and Bias. *Biophys. J.* **2003**, *84* (3), 2030−2042.
(31) Gouda, H.; Torigoe, H.; Saito, A.; Sato, M.; Arata, Y.; Shimada, I. Three-Dimensional Solution Structure of the B Domain of Staphylococcal Protein A: Comparisons of the Solution and Crystal Structures. *Biochemistry* **1992**, *31* (40), 9665−9672.
(32) Oikawa, H.; Suzuki, Y.; Saito, M.; Kamagata, K.; Arai, M.; Takahashi, S. Microsecond Dynamics of an Unfolded Protein by a Line Confocal Tracking of Single Molecule Fluorescence. *Sci. Rep.* **2013**, *3*, No. 2151.
(33) Otosu, T.; Ishii, K.; Oikawa, H.; Arai, M.; Takahashi, S.; Tahara, T. Highly Heterogeneous Nature of the Native and Unfolded States of the B Domain of Protein A Revealed by Two-Dimensional Fluorescence Lifetime Correlation Spectroscopy. *J. Phys. Chem. B* **2017**, *121* (22), 5463−5473.
(34) Nüesch, M. F.; Ivanović, M. T.; Claude, J. B.; Nettels, D.; Best, R. B.; Wenger, J.; Schuler, B. Single-Molecule Detection of Ultrafast BioMolecular Dynamics with Nanophotonics. *J. Am. Chem. Soc.* **2022**, *144* (1), 52−56.

https://doi.org/10.1021/acsphyschemau.3c00040
ACS Phys. Chem Au 2024, 4, 85−93